3D-Printed Silicone Soft Architectures with Programmed Magneto-Capillary Reconfiguration

Sangchul Roh, Lilian B. Okello, Nuran Golbasi, Jameson P. Hankwitz, Jessica A.-C. Liu, Joseph B. Tracy, Orlin D. Velev*

S. Roh, L. B. Okello, N. Golbasi, Prof. O. D. Velev
Department of Chemical and Biomolecular Engineering, North Carolina State University, Raleigh, NC 27695, USA
E-mail: odvelev@ncsu.edu
J. P. Hankwitz, J. A.-C. Liu, Prof. J. B. Tracy
Department of Materials Science and Engineering, North Carolina State University, Raleigh, NC 27695, USA

[REVISED Version. Please note TOC and TOC caption at the end]

Soft intelligent structures that are programmed to reshape and reconfigure under magnetic field can find applications such as in soft robotics and biomedical devices. We report a new class of smart elastomeric architectures that undergo complex reconfiguration and shape change in applied magnetic fields, while floating on the surface of water. These magnetoactive soft actuators are fabricated by 3D printing with homocomposite silicone capillary ink. The ultrasoft actuators easily deform by the magnetic force exerted on carbonyl iron particles embedded in the silicone, as well as lateral capillary forces. The tensile and compressive moduli of the actuators are easily determined by their topological design through 3D printing. As a result, their responses can be engineered by the interplay of the intensity of the magnetic field gradient and the programmable moduli. 3D printing allows us to fabricate soft architectures with different actuation modes, such as isotropic/anisotropic contraction and multiple shape changes, as well as functional reconfiguration. Meshes that reconfigure in magnetic fields and respond to external stimuli by reshaping could serve as active tissue scaffolds for cell cultures and soft robots mimicking creatures that live on the surface of water.

Soft material architectures that respond to external stimuli are of special interest for next-generation robotics and health care devices.[1–11] While a number of methods for making responsive materials have been reported, 3D printing is one of the most efficient fabrication techniques, due to its inherent rapid prototyping capabilities.[12–17] 3D-printed soft materials can exhibit complex responses by being actuated by several external stimuli, including solvents, electric fields, magnetic fields, and catalytic reactions.[12,14,16,18]

Magnetic fields enable remote, rapid stimulation of soft actuators containing magnetically active domains. These domains commonly contain magnetic particles, embedded in a soft matrix, such as hydrogel or elastomer.[7,8,16,19–22] Under applied magnetic fields, magnetic torques and/or forces are exerted on the magnetic particles, resulting in bulk deformation of the soft matrix in which they are embedded. In the case of magnetic torque, anisotropic magnetic domains generally tend to align along the direction of a uniform magnetic field because of shape anisotropy or interparticle interactions within chains, thus enabling deformation in multiple programmable configurations.[7,8,16,19–21,23] Even though external magnetic field gradients may generate strong structural responses, the task of designing soft actuators with multidirectional reconfiguration by magnetic field gradient force is challenging, because polarizable magnetic domains without residual magnetism in the matrix are attracted in the sole direction of the positive magnetic field gradient.[20,24,25]

Here, we demonstrate a new class of magneto-capillary 3D-printed soft actuators floating on water, which are multidirectionally responsive to simple vertical magnetic gradients. The actuators are composed of silicone-iron particle composite filaments fabricated by a method for 3D printing by direct extrusion of soft silicone paste that we reported earlier.[17] The filaments are shaped in the form of ultrasoft wavy structures (Figure 1(a)).[13,26,27] Such structures can readily deform under the combined action of the applied magnetic field and capillarity. We call the 3D-printed architecture consisting of wavy filaments an "elastin-like" mesh. Our strategy for making programmable and multidirectionally responsive materials is to

endow 3D-printed meshes with topological and spatial variations in the softness of the comprising filaments of the elastin-like meshes. These meshes are suspended on an air/water interface, which allows frictionless responses, mediated by the lateral capillary forces at the interface as well as lateral magnetic translational forces. We demonstrate multiple shape morphing and functional actuation capabilities as proof-of-concept examples, including an extending grabber on water, and a magnetically operated liquid droplet dispenser.
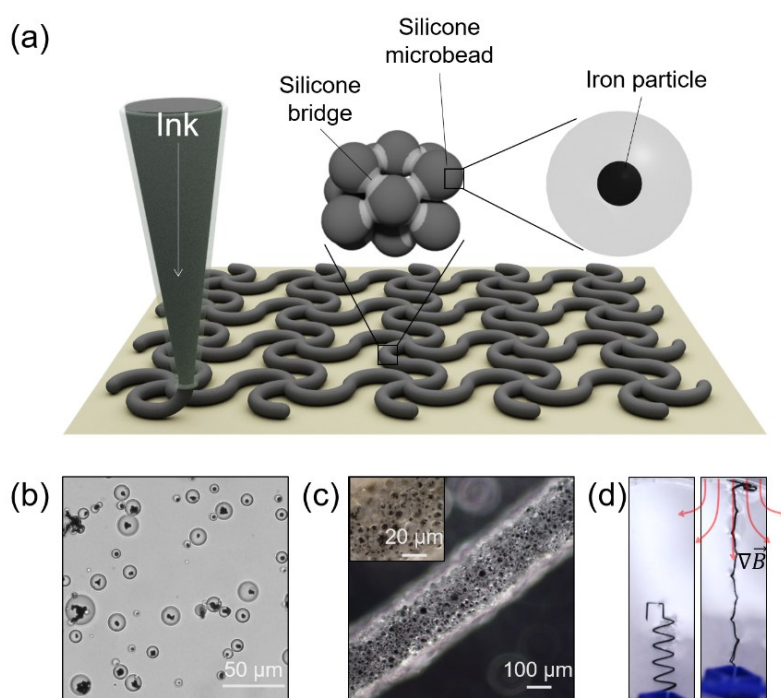

Figure 1. (a) Schematic of 3D printing via homocomposite capillary pastes. (b) Optical micrograph of PDMS microbeads containing 20 wt.% of magnetic particles. (c) A 3D-printed homocomposite capillary paste filament. The filament was ejected from a 27-gauge nozzle. (d) Example of a 3D-printed and crosslinked filament floating on water, that can be stretched by an applied magnetic field gradient.

A schematic of the method used for 3D printing of the magnetic actuator is illustrated in Figure 1(a). The magnetic inks for the direct extrusion writing were based on polydimethylsiloxane (PDMS) homocomposite capillary pastes (HCPs).[17] The HCP is composed of 70 wt.% of crosslinked PDMS microbeads containing 20 wt.% magnetic particles (Figure 2(b)), and 30 wt.% of PDMS precursor (capillary binder, liquid phase). We used commercially available 4 μm carbonyl iron particles with high saturation magnetization and lack of magnetic hysteresis. (Figure S1). The uncrosslinked PDMS precursor behaves as a

capillary binder that consolidates the PDMS beads into paste. The HCPs are prepared with water as an internal run-off phase. The mixture has thixotropic properties characterized by a shear-dependent liquid-to-solid transition, which enables direct ink writing (Video S1).[17] The HCP is extruded into filament-like structures (Figure 1(c)) and further crosslinked in an oven at 80 °C. Once crosslinked, the HCP retain their shape indefinitely. The PDMS HCP is especially well suited for 3D printing soft materials because the shaped and cured PDMS HCPs are similar to, or softer than, bulk pure PDMS. Other thixotropic PDMS pastes contain a large fraction of hard rheology modifiers such as fumed silica, which can cause extra hardening of the PDMS after curing.[17] The soft and elastic 3D-printed and crosslinked HCP filaments are hydrophobic and can readily float on the surface of water. They can be extended with a magnetic field gradient and return to the original shape after the magnetic field is removed due to the elasticity of the silicone mesh (Figure 1(d)).

3D printing of HCP by extrusion is a simple and versatile method for fabricating magneto-capillary actuators. Their design is inspired by the natural wavy and fibrous biomaterials, including collagen, elastin, and keratin.[13,26] These fibrous biopolymers are coiled and form tangled networks that enable a low-modulus response to relatively small stresses induced by a tensile load.[26] We fabricated magnetoactive soft meshes comprising elastin-like structures by printing HCP filaments with imbedded magnetic particles. The filaments overlap orthogonally at each intersection to form two-dimensional architectures (elastin-like mesh, Figure 1(a)). The structures were made of four overlaid layers of filament ejected from a conical printing nozzle (27-gauge) at ~ 60 psig with a printing nozzle speed of ~ 0.42 cm sec^{-1}.
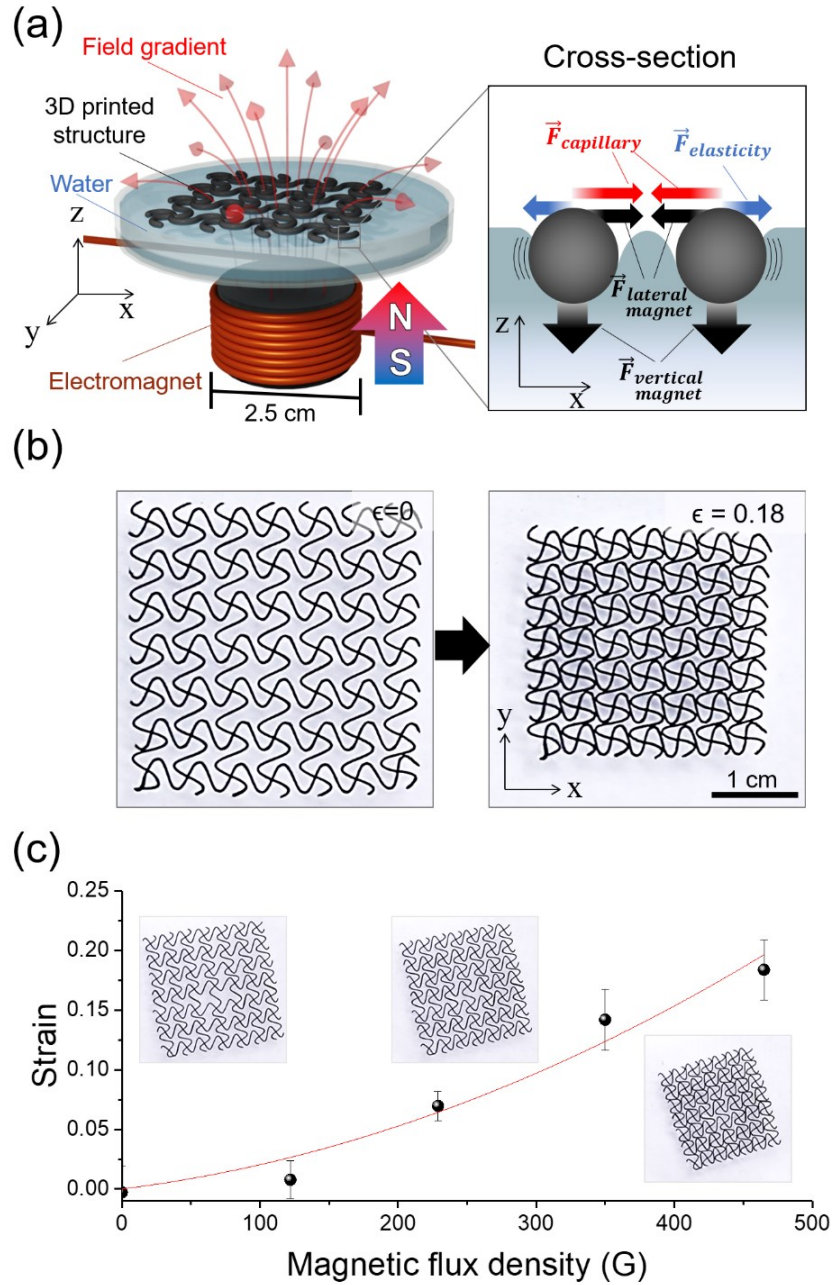
Figure 2. (a) Schematic of experimental setup for magnetic actuation (left) and forces exerted on a magnified part of the 3D-printed filament by an external magnetic field (right). (b) Photographs of 3D-printed magnetic mesh on water without (left) and with (right) an external magnetic field (real image, top-view). (c) The change in strain of the magnetic mesh (-$\Delta L/L_0$, where L_0 is the initial length of the mesh, and -ΔL is $L - L_0$) in (b) correlated to the magnetic field flux density, $\vec{B}_z$ at the distance of 8 mm from the electromagnet.

We used the set-up illustrated in Figure 2(a) for the magnetic actuation of the floating 3D-printed elastin-like meshes. The meshes were suspended on the surface of water contained in an 8-mm deep vessel with an electromagnet located beneath it. The flotation on a water surface allows to achieve frictionless actuation without hysteretic effects. The magnetic mesh

was ~ 3.6 cm wide, which is larger in size than the diameter of the electromagnet (2.5 cm). In this actuation set-up, two forces exerted on the elastin-like mesh determine its behavior: 1) lateral magnetic force and 2) lateral capillary force. The lateral magnetic force is generated by the gradient of the vertical magnetic flux, $\vec{B}_z$, in the xy plane. $\vec{B}_z$ radially decreases with increase in the distance from the center of the electromagnet generating the magnetic field (See also Figure S2). Therefore, the mesh experiences a lateral magnetic force towards the center of the magnet on xy plane, where the field density is highest (Figure S2).

The meshes don't sink because the vertical magnetic force in the z-direction is balanced by the surface tension of water. The capillary length of the floating mesh is approximated by $q^{-1} = \left(\frac{\gamma}{\Delta\rho g}\right)^{\frac{1}{2}}$, where γ is the surface tension of water, $\Delta\rho$ is the density difference between water and air, g is the gravitational acceleration.[28] The approximate capillary length of the system is ~ 2.7 mm which is ~ 17-fold bigger than the diameter of the filaments (0.16 mm). Thus, the mesh that is pulled vertically towards the electromagnet and slightly submerged is subjected to lateral capillary forces that pull the filamentous structure together. The lateral capillary force is generated by the increased surface area of the air-water interface confined between the filaments.[29] The lateral capillary force between floating objects is proportional to the square of the density of the objects ($F_{capillary} \propto \rho_{mesh}^2$), where in our system the "apparent" density of the mesh could be evaluated by $\rho_{mesh} \propto \nabla(\vec{m} \cdot \vec{B})_z$ where $\vec{m}$ is the magnetic moment and $\vec{B}$ is the magnetic flux density.[29–31] An increase in the magnetic flux density increases both the lateral capillary force and lateral magnetic force (Figure S2 and Figure S3). The lateral capillary and lateral magnetic forces drive contraction of the magnetic mesh in the xy plane (Figure 2(b) and Video S2).

A reasonable parameter that could be varied and measured for understanding the behavior of the mesh is the z-directional magnetic flux density at 8 mm from the center of the electromagnet because it controls both the lateral capillary force and lateral magnetic force. The

horizontal dimensions of the mesh reduced as $\vec{B}_z$ gradually increased as the combined action of lateral capillary forces and magnetic force brought the filaments together (Figure 2(c)). At the highest value of $\vec{B}_z$ plotted in the graph of Figure 2(c), the mesh was fully closed (at $\epsilon \sim 0.18$, the filaments touch each other as shown in Figure 2(b) right). The compressive modulus of the mesh appears to dramatically increase after the structure fully closes. Upon turning off the electromagnet, the mesh floats up and rapidly returns to its initial shape (< 0.1 sec) due to the elasticity of the silicone filaments (Video S2).

We further investigated how the shape responses of the floating magnetic meshes can be programmed by controlling the spatial variations in their softness. The softer segments on the mesh are expected to deform more than stiffer sections when pulled downwards by the same magnetic force. To prove this concept, we prepared elastin-like meshes consisting of filaments whose amplitude (A) and wavelength (λ) ratio (A/λ) are varied from 0 to 0.31 (Figure 3(a)). Here, the wavelength stands for the distance between successive crests of the wavy filaments as schematically defined in Fig.3(a). Initially, these meshes were ~3.6 cm wide without an applied magnetic field. After applying the field, all meshes compressed except for the mesh with $A = 0$. The meshes with higher A / λ exhibited larger deformation for the same applied magnetic field gradient (Figure 3(b)).

The dependence of the degree of deformation on the A / λ ratio and the intensity of the external magnetic field gradient enabled us to program their shape morphing in multiple ways. We prepared an anisotropic mesh composed of straight filaments along the y-axis and wavy filaments along the x-axis, shown in Figure 3(c). The A / λ ratio was 0.31, which is the same as the ratio of the isotropic mesh in Figure 3(a). When the same magnetic field gradient was applied as in Figure 3(a), the anisotropic mesh was compressed only along the x-axis (wavy filament) while there was negligible deformation along the y-axis (straight filaments), as shown in Video S3. Indeed, deformation along the x-direction is nearly superimposable with the wavy

mesh for which A / λ was 0.31 in both directions. These results prove that the response of the

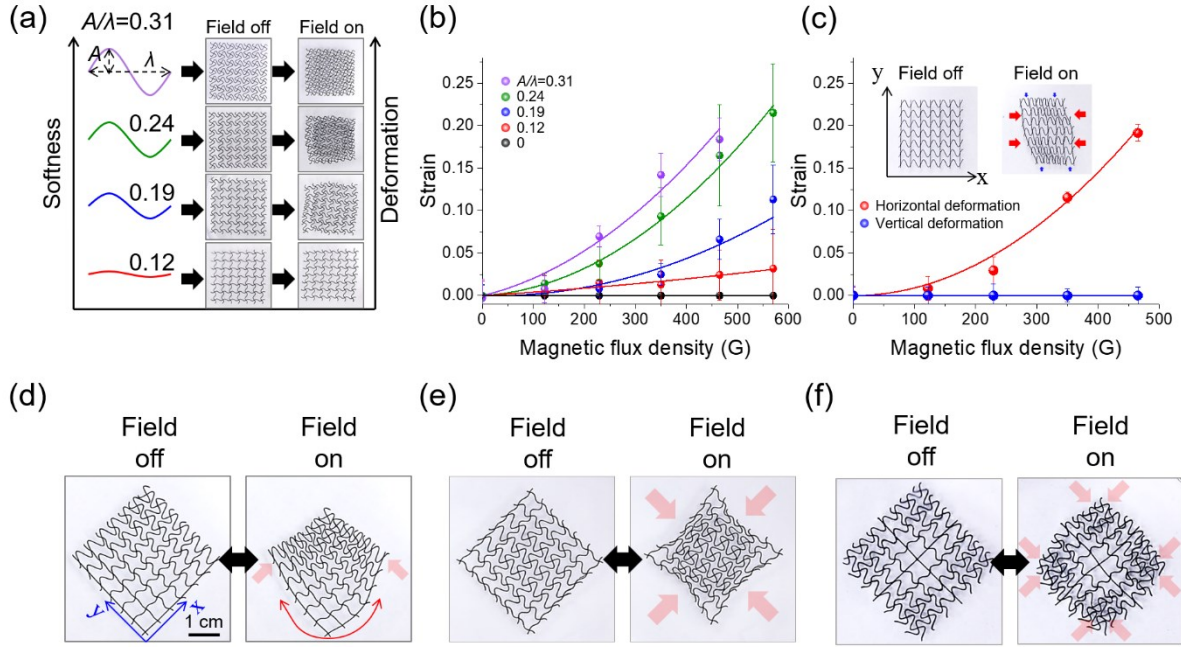magnetic soft meshes can be programmed by the spatial and topological variations of A / λ.

Figure 3. (a) Deformation of magnetic meshes as a function of changing A / λ. (b) Deformation of meshes with different A / λ ratios in response to the magnetic field gradient. (c) Deformation of an anisotropic mesh in varying magnetic field gradient. The red and blue lines indicate deformation along x-axis and y-axis, respectively. (d-f) Shape change with and without magnetic fields of meshes with (d) gradient pattern, (e) soft pattern in the center and (f) hard pattern in the center. The response can be reliably programmed by the wavy mesh period and amplitude.

Knowing how the spatial deformation depends on the softness of the filaments and the

A / λ ratio enables us to fabricate magnetic actuators with programmed shape changes. Three

different examples of the deterministic shape change with magnetic field gradient are shown in

Figure 3(d-f) and Video S4. Figure 3(d) shows a mesh which has a spatial gradient in A / λ ratio

from 0 to 0.37. Since the upper edge of the mesh is softer, it shrinks more with the magnetic

field at $\vec{B}_z = 570$ G. As a result, the whole structure bends in-plane towards the positive magnetic

field gradient on the xy plane. Furthermore, when filaments with higher A / λ ratios are localized

at the center of the mesh, only the center of the mesh compresses and the square mesh morphs

into a star shape (Figure 3(e)). Similarly, when the softer parts are localized at the edges of the square mesh, the sharp edges are blunted when the magnetic field is applied (Figure 3(f)).

The reversible, shape-dependent response of these soft meshes, described above, enables proof-of-concept demonstrations of soft robots with complex functions, such as a soft extending grabber that can extend and capture an object floating on water. The soft robot is composed of the anisotropic, elastin-like mesh and a gripper, shown in Figure 4(a) and Video S5. At an applied magnetic field of $\vec{B}_z$=570 G, the soft extending lattice on surface of water above the electromagnet contracted on xy plane, while the grabber at its end closed. Upon removing the magnetic field, the grabber extended towards the target object (a small ball of crumpled aluminum foil) and opened. Switching the magnetic field back on caused the grabber to close around the object an then pull it (Video S5). These results demonstrate the potential for applications of these 3D-printed magnetic materials in intelligent soft actuators and robots interacting with objects on water surfaces.
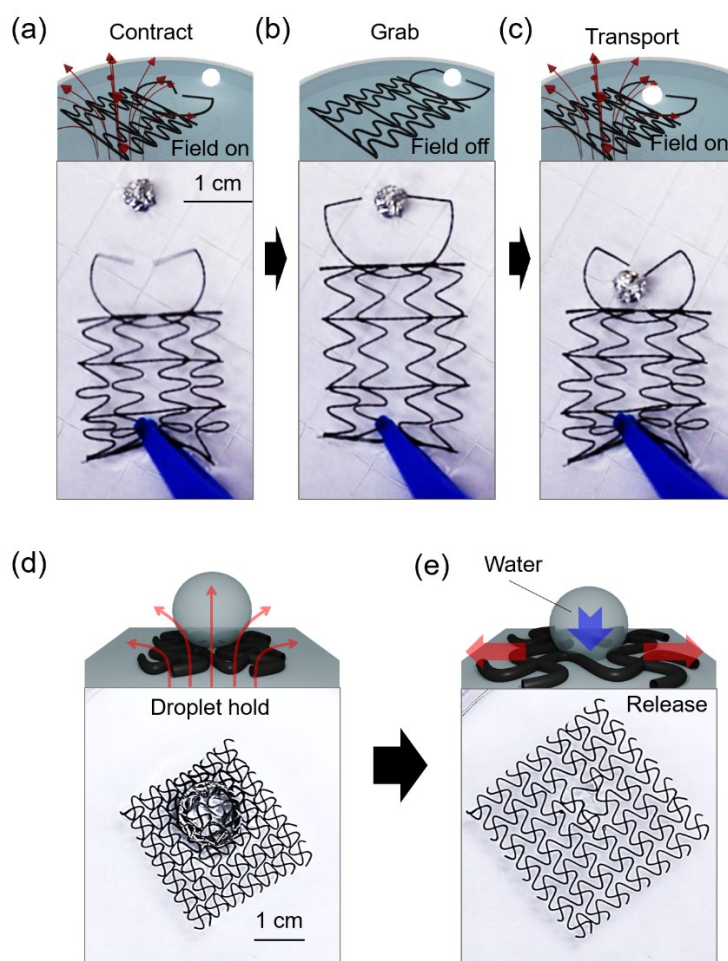
Figure 4. (a-c) Extensible surface grabber that operates in three phases: (a) Contraction of the filaments and closing the grabber. (b) Opening the end and extension toward the object by switching off the magnetic field. (c) Grabbing by turning on the magnetic field, which also transports the object. (d,e) Magnetically responsive water droplet dispenser: (d) The droplet is held on top of the mesh when it is closed by the applied magnetic field; (e) Upon removing the magnetic field, the mesh is opened and the water droplet is released and penetrates through the mesh.

As another example of an application, we further demonstrated the capability of our 3D-printed materials as a magnetically switchable water droplet dispenser in Figure 4(d) and Video S6. When the 3D-printed architecture in Figure 4(d) is fully contracted with the magnetic field, the hydrophobicity of the mesh (contact angle = 116°) as well as the small gap between filaments enables a water droplet to freely stand on the mesh by preventing it from penetrating through the gap as shown in Figure 4(e). Upon switching off the magnetic field, the gap between the 3D-printed filaments increases, allowing the water droplet to merge and mix with the other water phase. Similar functionality could enable applications in droplet microfluidics and future smart devices for drug release.

In summary, we present a class of versatile, 3D-printed, magnetic meshes made using homocomposite capillary ink containing iron microparticles. They can be actuated through the use of magnetic forces, mediated by capillarity, while floating on water. These magnetic actuators are reversibly laterally contracted and expanded by controlling the normal magnetic field applied from below the vessel. Their targeted shape change can be programmed by engineering the pattern of the filamentous mesh. The 3D printing method with multiphasic capillary paste is well suited for making 3D structures as described in our previous publication.[17] However, here we have focused on the distinct simple and efficient system of magnetic mesh floating on the surface of water. This allows for actuation by use of a single electromagnet, where the magnetic force responsible for actuation in this work is lateral rather than vertical. Future research in such structures may entail the making of intelligent, multi-responsive, 2D and 3D magentoactive materials and devices. This new class of magnetoactive actuators enabled by this 3D printing technique enables fabrication of a with potential applications, spanning active tissue scaffolds for cell cultures and various types of soft robots mimicking creatures that live on the surface of water.

Experimental Section

Fabrication of PDMS Homocomposite Capillary Pastes (HCPs): Beads of PDMS with embedded magnetic particles (m-PDMS) were fabricated by emulsifying a mixture of 20 wt.% carbonyl iron microparticle with an average diameter of 4.2 μm (MMPs, Jilin Jien Nickel Industry, JCF2-2) in PDMS prepolymer (Sylgard 184, Dow chemical) in 10 wt.% of polyvinyl alcohol (Mowiol 18-88, Sigma Aldrich) aqueous solution. The base to curing agent mixing ratio was 20:1. For emulsification, we used a benchtop ServoDyne mixer (Cole-Parmer) equipped with an impeller (three blades of 1 cm) at 1000 rpm. The emulsion was then placed in an oven overnight to crosslink the PDMS microbeads at 60 °C. The microbeads were further rinsed with 0.1 wt.% of Tween 20 aqueous solution 10 times to remove the residual polyvinyl alcohol. After every rinsing cycle of the PDMS microbeads, the PDMS beads were collected using a permanent magnet. The PDMS beads in water suspension was further mixed with uncrosslinked PDMS precursor (40:1 = base:curing agent) to make the homocomposite capillary pastes using the ServoDyne mixer.

Manipulation of 3D printed meshes on water with an electromagnet: We filled a disposable petri dish with Millipore in which that the depth of water was 8 mm for all manipulations. An electromagnet (Uxcell, 12V DC, 800 N capacity) was placed beneath of the center of the disposable petri dish. The electromagnet was connected to a DC power supply (EXTECH® Instruments) of which voltage can be controlled. To measure the magnetic flux density of the electromagnet by changing the distance from the electromagnet, we used a Gaussmeter (AlphaLab Inc. Model GM-2). The changes in the shape of the meshes on water surface were measured in in the digital frames using ImageJ software (National Institutes of Health). To measure the contact angle of the water droplet (100 μl), it was placed on the magnetic mesh and the image of the drop was recorded with a digital camera (Canon EOS 5D Mark II). The contact angle was analyzed with imageJ software.

Characterization of the magnetic properties of Homocomposite Capillary Inks: A Quantum Design MPMS 3 SQUID/VSM magnetometer was used to measure the magnetization curve of the HCPs at 300 K.

3D Printing: The 3D printer was built using the design of a CNC (computer numerical control) mini-mill from OpenBuilds, which was customized to move a Nordson EFD syringe barrel rather than the typical CNC spindle for which the machine was designed. Pneumatic pressure is regulated by a Performus V Fluid Dispenser and delivered to the syringe barrel to provide controlled extrusion through a 27-gauge polyethylene nozzle. Movement in the x, y, and z directions is controlled by an Arduino Mega 2560 microcontroller board equipped with a Ramps 1.4 driver board.

References

[1]   X. Zhao, J. Kim, C. A. Cezar, N. Huebsch, K. Lee, K. Bouhadir, D. J. Mooney, *Proc. Natl. Acad. Sci.* **2011**, *108*, 67.
[2]   I. C. Kwon, Y. H. Bae, S. W. Kim, *Nature* **1991**, *354*, 291.
[3]   H. Masoud, B. I. Bingham, A. Alexeev, *Soft Matter* **2012**, *8*, 8944.
[4]   R. F. Shepherd, F. Ilievski, W. Choi, S. A. Morin, A. A. Stokes, A. D. Mazzeo, X. Chen, M. Wang, G. M. Whitesides, *PNAS* **2011**, *108*, 20400.
[5]   M. M. Schmauch, S. R. Mishra, B. A. Evans, O. D. Velev, J. B. Tracy, *ACS Appl. Mater. Interfaces* **2017**, *9*, 11895.
[6]   S. K. Smoukov, S. Gangwal, M. Marquez, O. D. Velev, *Soft Matter* **2009**, *5*, 1285.
[7]   B. Bharti, A.-L. Fameau, M. Rubinstein, O. D. Velev, *Nat. Mater.* **2015**, *14*, 1104.

[8]   W. Hu, G. Z. Lum, M. Mastrangeli, M. Sitti, *Nature* **2018**, *554*, 81.
[9]   D. Morales, E. Palleau, M. D. Dickey, O. D. Velev, *Soft Matter* **2014**, *10*, 1337.
[10]   L. Ionov, *Adv. Funct. Mater.* **2013**, *23*, 4555.
[11]   X. He, C. Li, F. Chen, G. Shi, *Adv. Funct. Mater.* **2007**, *17*, 2911.
[12]   A. S. Gladman, E. A. Matsumoto, R. G. Nuzzo, L. Mahadevan, J. A. Lewis, *Nat. Mater.* **2016**, *15*, 413.
[13]   A. Clausen, F. Wang, J. S. Jensen, O. Sigmund, J. A. Lewis, *Adv. Mater.* **2015**, *27*, 5523.
[14]   M. Wehner, R. L. Truby, D. J. Fitzgerald, B. Mosadegh, G. M. Whitesides, J. A. Lewis, R. J. Wood, *Nature* **2016**, *536*, 451.
[15]   D. Kokkinis, M. Schaffner, A. R. Studart, *Nat. Commun.* **2015**, *6*, 8643.
[16]   Y. Kim, H. Yuk, R. Zhao, S. A. Chester, X. Zhao, *Nature* **2018**, *558*, 274.
[17]   S. Roh, D. P. Parekh, B. Bharti, S. D. Stoyanov, O. D. Velev, *Adv. Mater.* **2017**, *29*, 1701554.
[18]   D. Han, C. Farino, C. Yang, T. Scott, D. Browe, W. Choi, J. W. Freeman, H. Lee, *ACS Appl. Mater. Interfaces* **2018**, *10*, 17512.
[19]   S. R. Mishra, M. D. Dickey, O. D. Velev, J. B. Tracy, *Nanoscale* **2016**, *8*, 1309.
[20]   J. Kim, S. E. Chung, S.-E. Choi, H. Lee, J. Kim, S. Kwon, *Nat. Mater.* **2011**, *10*, 747.
[21]   K. Han, C. W. Shields IV, N. M. Diwakar, B. Bharti, G. P. López, O. D. Velev, *Sci. Adv.* **2017**, *3*, e1701108.
[22]   G. Z. Lum, Z. Ye, X. Dong, H. Marvi, O. Erin, W. Hu, M. Sitti, *Proc. Natl. Acad. Sci.* **2016**, *113*, E6007.
[23]   R. M. Erb, J. J. Martin, R. Soheilian, C. Pan, J. R. Barber, *Adv. Funct. Mater.* **2016**, *26*, 3859.
[24]   P. Garstecki, P. Tierno, D. B. Weibel, F. Sagués, G. M. Whitesides, *J. Phys. Condens. Matter* **2009**, *21*, 204110.
[25]   S. H. Kim, J. Y. Sim, J. M. Lim, S. M. Yang, *Angew. Chemie* **2010**, *122*, 3786.
[26]   K.-I. Jang, H. U. Chung, S. Xu, C. H. Lee, H. Luan, J. Jeong, H. Cheng, G.-T. Kim, S. Y. Han, J. W. Lee, J. Kim, M. Cho, F. Miao, Y. Yang, H. N. Jung, M. Flavin, H. Liu, G. W. Kong, K. J. Yu, S. I. Rhee, J. Chung, B. Kim, J. W. Kwak, M. H. Yun, J. Y. Kim, Y. M. Song, U. Paik, Y. Zhang, Y. Huang, J. A. Rogers, *Nat. Commun.* **2015**, *6*, 6566.
[27]   E. Munch, M. E. Launey, D. H. Alsem, E. Saiz, A. P. Tomsia, R. O. Ritchie, *Science* **2008**, *322*, 1516.
[28]   P. A. Kralchevsky, K. Nagayama, *Langmuir* **1994**, *10*, 23.
[29]   P. A. Kralchevsky, N. D. Denkov, *Curr. Opin. Colloid Interface Sci.* **2001**, *6*, 383.
[30]   O. D. Velev, N. D. Denkov, V. N. Paunov, P. A. Kralchevsky, K. Nagayama, *Langmuir* **1993**, *9*, 3702.
[31]   O. T. Mefford, R. C. Woodward, J. D. Goff, T. P. Vadala, T. G. St. Pierre, J. P. Dailey, J. S. Riffle, *J. Magn. Magn. Mater.* **2007**, *311*, 347.

Supporting Information
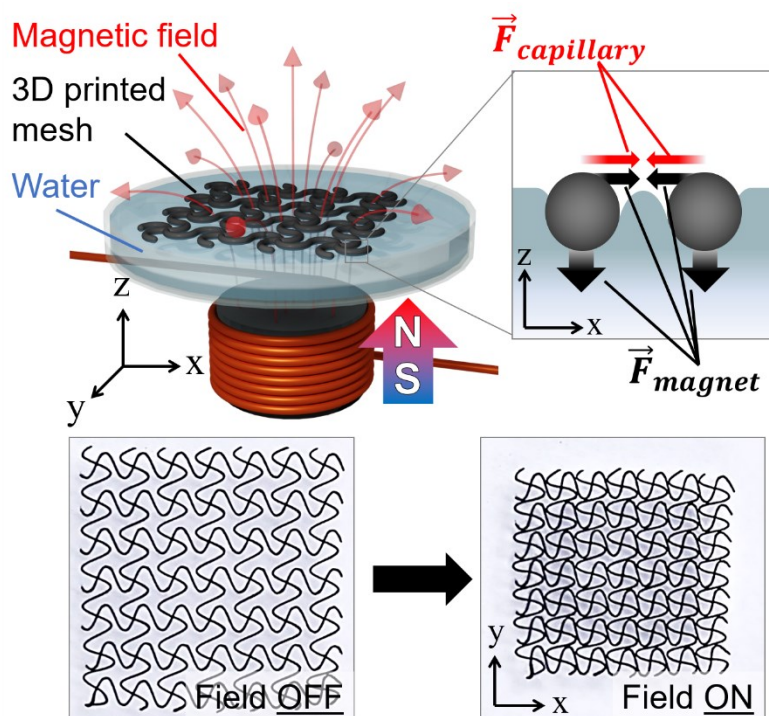Supporting Information is available from the Wiley Online Library or from the author.

Table of contents entry

A new class of soft 3D-printed actuators and meshes with magnetic response is presented. They are made of homocomposite silicone capillary ink containing iron microparticles. They are floating on water and are actuated via magnetic field mediated by capillarity. Their response and reconfiguration pattern are programmed by the pattern of the filaments.